Title

The Effect of Kinematical Parameters and Tool Geometry on Burr Height in Face Milling of Al-Si Alloys

Authors

Avila, Miguel C.
Dornfeld, David A

Publication Date

2003-06-01

The Effect of Kinematical Parameters and Tool Geometry on Burr Height in Face Milling of Al-Si Alloys

Miguel C. Avila
Sponsored by CODEF

Abstract— High speed face milling test were performed on two aluminum silicon alloys currently used in automotive engine production to study the effect of cutting parameters and tool geometry in edge quality. Axial Rake and Radial Rake angles were varied to assess their effect in burr formation, as well as cutting speed, feedrate and depth of cut. Significant improvements in edge quality were obtained by optimizing these geometrical and kinematical parameters.

Keywords: aluminum, silicon, face milling, burr, deburring, metal cutting, radial, axial rake, lead, angle, speed, feed rate.

1. Introduction

Face milling is among the most ubiquitous material removal processes in industry. The face milling operation is, however, accompanied by burr formation. Edge-breakouts are also formed in brittle materials. Nowadays, as the complexity of finished products and the stringency of dimensional tolerances increase, edge finishing is paramount. In consequence, it is usually necessary to recur to non-productive, non-value-added deburring operations that have a negative impact in production costs and lead times. It is then desirable to minimize, and if possible prevent, burr formation associated with the machining processes. In this realm, the study of burr prevention strategies is particularly attractive.

Kinematical and geometrical strategies for burr minimization involve optimization of the following : cutting parameters, namely cutting speed, feedrate and depth of cut; tool path; and tool geometry, defined by axial rake, radial rake and lead angles. In this study, cutting parameters and tool geometry are considered, and their effect in burr height and thickness was assessed in two aluminum-silicon alloys, AlSi7Mg-wa and Alsi9Cu3. This family of alloys has seen increased usage in recent years, as they are finding their way into new, high-volume applications in automotive production; for example: engine cylinder heads, and more recently, engine blocks and chassis components. Al-Si alloys offer high specific strength and modulus of elasticity, easy recycling, and have relatively low costs; however, the hard silicon grains accelerate tool wear, and frequent insert changeovers are often required to keep burr size within tolerance.

In a milling operation, the direction of chip flow is closely related to burr formation. Based on this observation, Exit Order Sequence Theory (EOS) has been proposed to

predict burr size on the exit surface [1]. EOS considers the three-dimensional chip-flow characteristics of the work material, associated with the order in which the major and minor cutting tool edges exit the workpiece, Tool geometry, feedrate, and depth of cut govern the exit order of the cutting edges. Under the assumption that the tool tip radius is smaller than the uncut chip thickness, if the minor cutting edge A-B exits the workpiece sooner than the major cutting edge B-C, the chip hinges on the transition surface, and a side burr is formed (Figure 1). On the contrary, if A-B exits the workpiece later than B-C, the chip hinges on the machined surface, and an exit burr is formed. As the transition surface is removed during subsequent cutting passes, and exit burrs on the machined surface are our main concern, the preferred Exit Order Sequence is A-B-C.

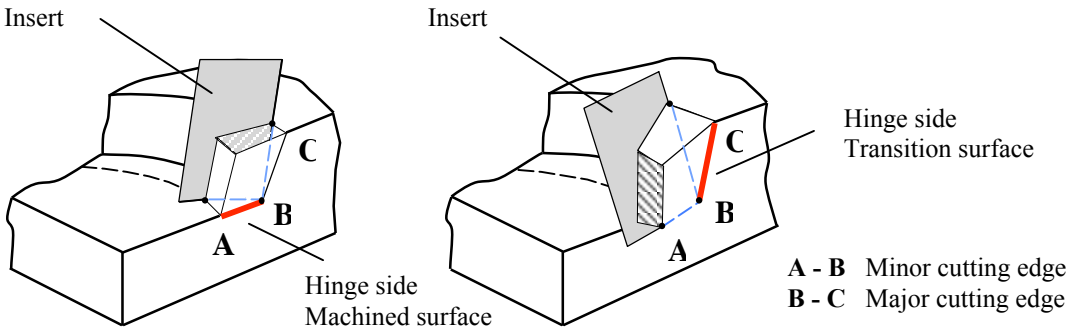

Figure 1. Schematic view of idealized tool edge exit order and resulting chip flow characteristics.

2. Experimental framework

Face milling cutting tests were performed on AlSi9Cu3 and AlSi7Mg-wa alloy blocks using a 125 mm diameter mill. Some mechanical properties of the alloys tested are displayed in Table 1. The feed direction was normal to the edges, as shown in Figure 2. Table 2 shows the cutting parameters used. A single, worn Kieninger Polycrystalline Diamond insert with a nose chamfer of 0.41 mm was used throughout the tests; the insert was taken from an automotive engine-block production line that had seen approximately 50×10^3 cuts (Figure 3). Radial rake and axial rake angles of the tool were modified with the aid of mounting brackets. Table 3 indicates the tool geometries tested. Lead angle was fixed at 90°, due to its weak effect in burr size and surface roughness [2]. An Ex-Cell-O high-speed, three-axis CNC machining center was used to conduct the experiments.

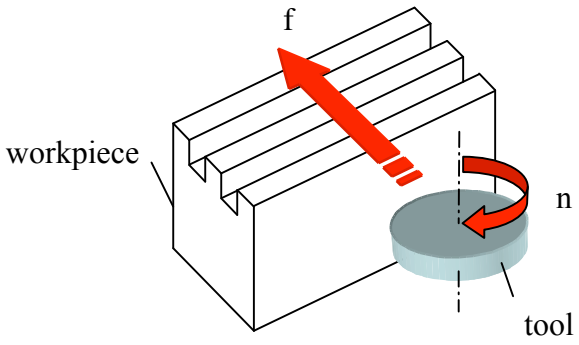

Figure 2. Schematic view of workpiece geometry and test configuration. 2 slots were pre-machined in order to obtain two replications per experiment.

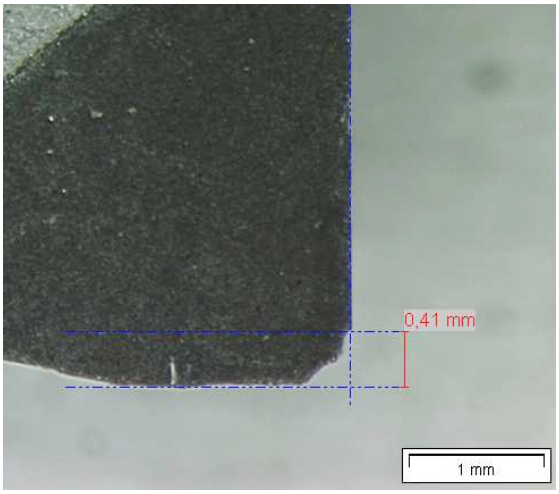

Figure 3. PKD diamond insert used.

Table 1. Silicon content and mechanical properties of the alloys tested. Average values DIN 1725 T.2.

Material	Si Content (%)	E (GPa)	S_y (MPa)	S_u (MPa)	A5 %
AlSi9Cu3	9	71	125	180	2
AlSi7Mg-wa	7	70	255	280	4.5

Table 2. Cutting conditions.

Spindle Speed **n** (min^{-1})	Cutting Speed $\mathbf{V_c}$ (m/min)
3200	1257
6400	2513
10000	3927

Feed per tooth $\mathbf{f_z}$ (mm)
0.08
0.14

Depth of cut **doc** (mm)
0.80
1.20
1.50

Table 3. Tool geometries tested.

Axial rake angle (α) (degrees)	Radial rake angle (β) (degrees)	Lead angle (γ) (degrees)
(0,	4,	90)
(4,	0,	90)
(6,	0,	90)
(6,	-6,	90)

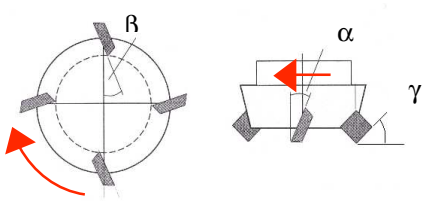

Burr height and thickness were measured using a microscope and CCD camera setup driven by AnalySIS digital image analyzing software. In a previous study of face milling of aluminum alloys by Bansal and Lee [2], it was shown that burr height is proportional to burr thickness; thereby burr thickness was measured only on AlSi7Mg wa workpieces for verification purposes. The results agreed with Bansal and Lee's study regarding the burr height-burr thickness proportionality.

3. Results and Discussion

3.1 EOS prediction

The different exit order sequences corresponding to the cutting conditions and tool geometries tested are depicted in Figure 4. Possible exit orders with increasing burr size are ABC, BAC, ACB, BCA, CAB, and CBA. Based on the exit orders given by the simulation, the following observations can be made. Smaller burrs are expected to occur in regions farther away from the tool center, or in other words, burr size decreases with increasing in-plane exit angle (from 90° to 180°). With regard to tool geometry, positive axial rake angles produce smaller burrs than negative (or neutral) angles, and negative radial rake angles produce smaller burrs than positive (or neutral) angles. On the other hand, exit orders improve with decreasing federate and with increasing depths of cut.

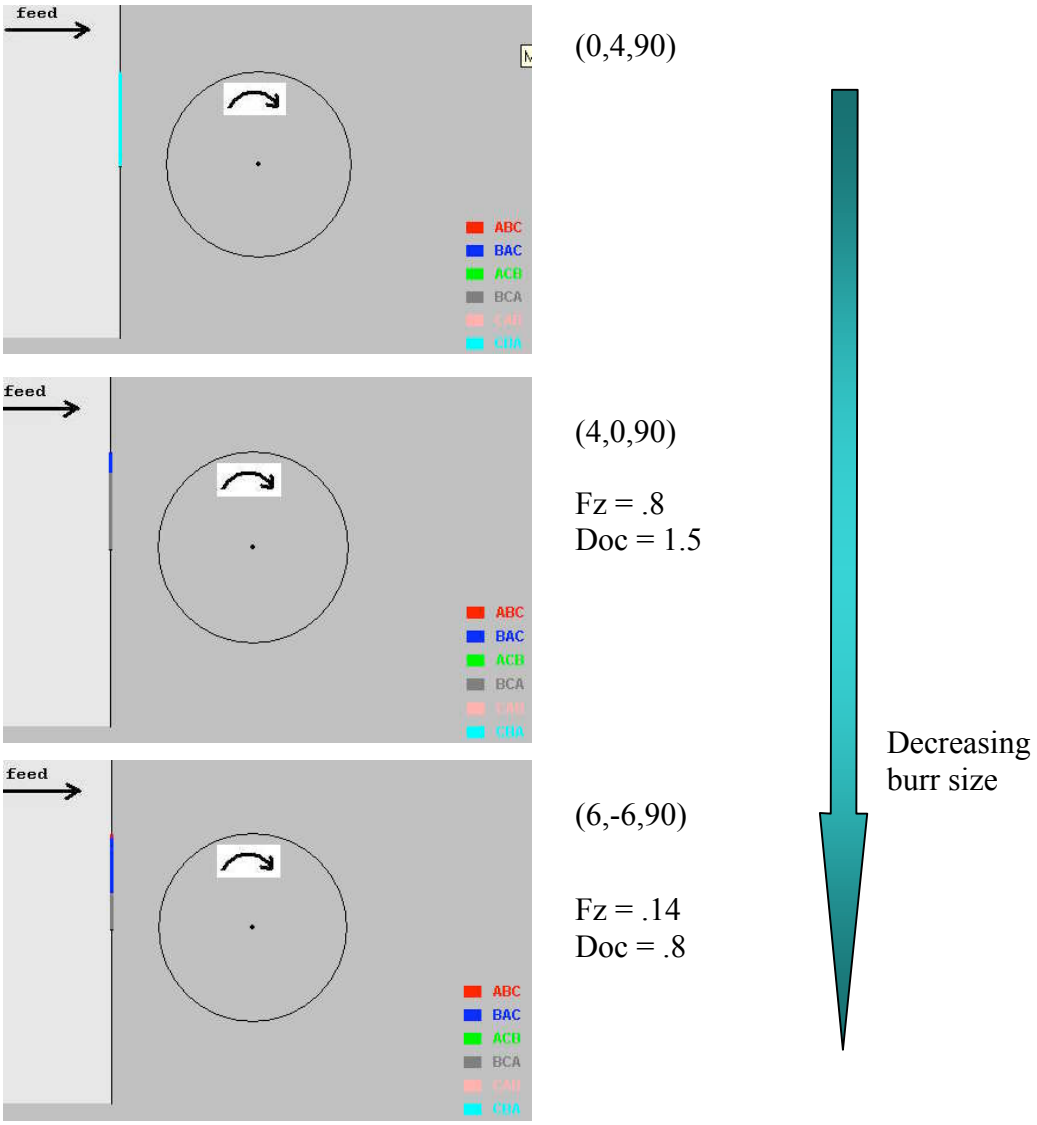

Figure 4. EOS prediction for various tool geometries and cutting conditions. Screenshots are from JAVA applet developed by Bansal [3].

3.2. Types of Milling Burrs observed

Different kinds of burrs were observed in the Al-Si alloys studied, and their occurrence was clearly dominated by the material properties. Table 1 lists the most important bulk mechanical properties of AlSi9Cu3 and AlSi7Mg alloys. The former alloy is roughly twice as ductile as the latter (as indicated by A5% elongation figures), mainly due to their disparate Si contents. Similarly, as indicated by the yield and ultimate strengths values, AlSi7Mg wa is significantly tougher and can absorb more plastic strain energy. Not surprisingly, the burr height observed on AlSi7Mg was, for all conditions, at least 20% greater, and edge breakouts appeared on AlSi9Cu3, as this material is more brittle. Contrariwise, no edge break-outs were observed in AlSI7Mg-wa.

Figure 5a shows a typical burr obtained on AlSi9Cu3. Using the burr classification scheme proposed by Hashimura et al. [1], these can be categorized as discontinuous, ductile plus fracture type burrs. In terms of their shape (macro-view), the burrs observed do not show geometrical continuity along a distance greater than the undeformed chip thickness of one tool pass. In terms of the formation mechanism, numerous edge breakouts were observed; in fact, on AlSi9Cu3, edge breakouts (negative burrs) were more frequent and generally larger than the accompanying burrs. On the contrary, edge breakouts were not observed on AlSi7Mg-wa (Figure 5b). In this case, the burrs observed were continuous, fracture plus ductile type. The burrs displayed, essentially, constant height and thickness across the center portion of the edge (in-plane exit angles between

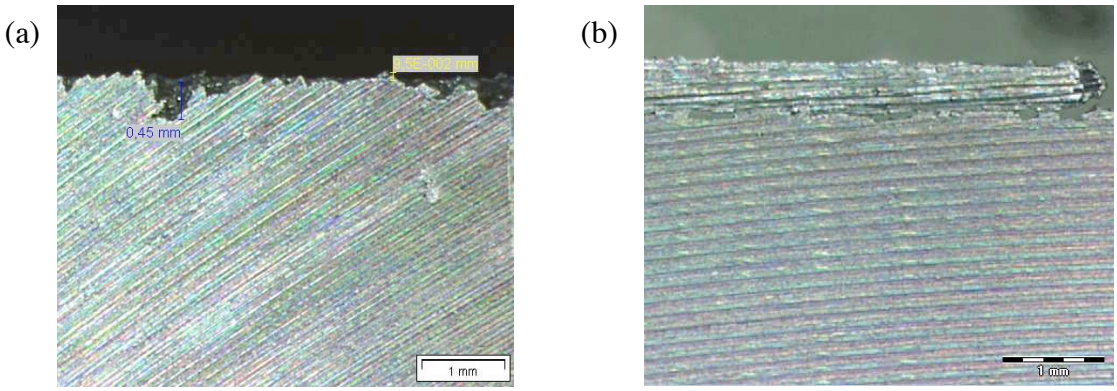

Figure 5. Typical burrs observed in AlSi7Mg-wa (a), AlSi9Cu3 (b).

approximately 160° and 200°), including tool exit and entrance. These burrs can also be classified as knife-type [4] due to their continuous, laminar shape. Their height was approximately equal to the depth of cut, suggesting that the mechanism of formation is similar to that of Rollover burrs in orthogonal cutting proposed by Gillespie [4]. In this case, the last remaining uncut chip before the tool exits the workpiece (at in-plane exit angle of 180°), is bent or pushed by the mayor cutting edge before it can be cut by the minor cutting edge. As a result, the chip continues to propagate throughout the edge as the tool continues to push it in the feed direction. Longitudinal cracks were observed at the root of the burrs; in the regions close to the borders of the machined edge, the burrs fell off the workpiece and the fractured cross-section areas remained as "burr traces", or in other words, secondary burrs.

3.3. Effect of cutting parameters on burr and break-out height

Figure 6 shows the effect of cutting conditions on burr height of AlSi9Cu3 alloy, machined with tool geometry (0,4,90). The same pattern was observed on AlSi7Mg. Four observations can be derived from the graph. First, the response of burr height with respect to cutting speed is non-monotonic. From 1257 m/min to 2513 m/min, burr height increases, and then reduces to minimum levels at 3927 m/min. This behavior can be explained by a transition from ductile to fragile behavior above 2513 m/min. The shape

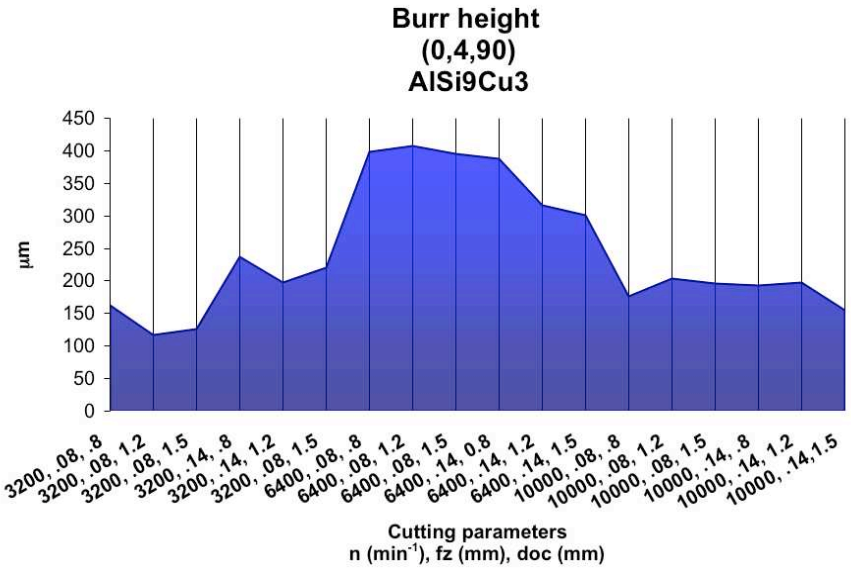

Figure 6. Exit burr height of AlSi9Cu3 milled with tool geometry (0,4,90), as a function of cutting conditions: spindle speed, feed per tooth and depth of cut.

of the burr height curve, in fact, has essentially the same shape as typical curves of ductility and energy required to fracture a specimen as a function of testing velocity. Thus, the critical velocity above which less energy is required to induce shearing (cutting), rather than bending, is close to 2513 m/min. Second, at the slowest cutting speed tested (1257 m/min), the response of burr height with respect to feedrate and depth of cut is very well defined. Burr height increases with feedrate, and decreases as depth of cut increases. Both results consist with EOS Theory prediction. It is to note, however, that between doc=0.8 mm and doc=1.5 mm, a minimum (optimum) depth of cut is observed. This result agrees with a similar study done by Bansal and Lee [2]. At a cutting

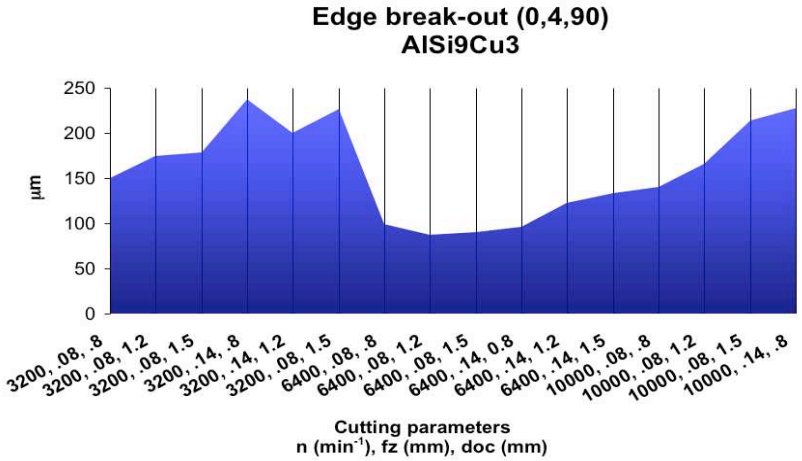

Figure 7. Exit break-out height of AlSi9Cu3 milled with tool geometry (0,4,90), as a function of cutting conditions: spindle speed, feed per tooth and depth of cut.

speed of 2513 m/min, burr height also decreases as depth of cut increases, but, conversely, burr height decreases as feed increases. Thirdly, the response of burr height as a function of feed and depth of cut is essentially flat at 3927 m/min. Under this regime, cutting speed is predominant, and the effect of other cutting parameters becomes weak.

Figure 7 shows break-out height as a function of cutting parameters. A drop in break-out size is observed at 2513 m/min, and it's due to an increase in ductility of the material. As mentioned previously, this regime may correspond to the critical velocity of ductile-fragile transition. It is also noted that the break-out curve closely resembles a mirror-image of the burr height curve. This observation suggests that for AlSi9Cu3, there is a compromise relationship burrs and break-outs. Regarding AlSi7Mg, as mentioned previously, no break-outs were observed.

3.4. Burr and break-out height distribution along the edge

Figure 8 shows a typical burr height and break-out height distribution on AlSi9Cu3. A

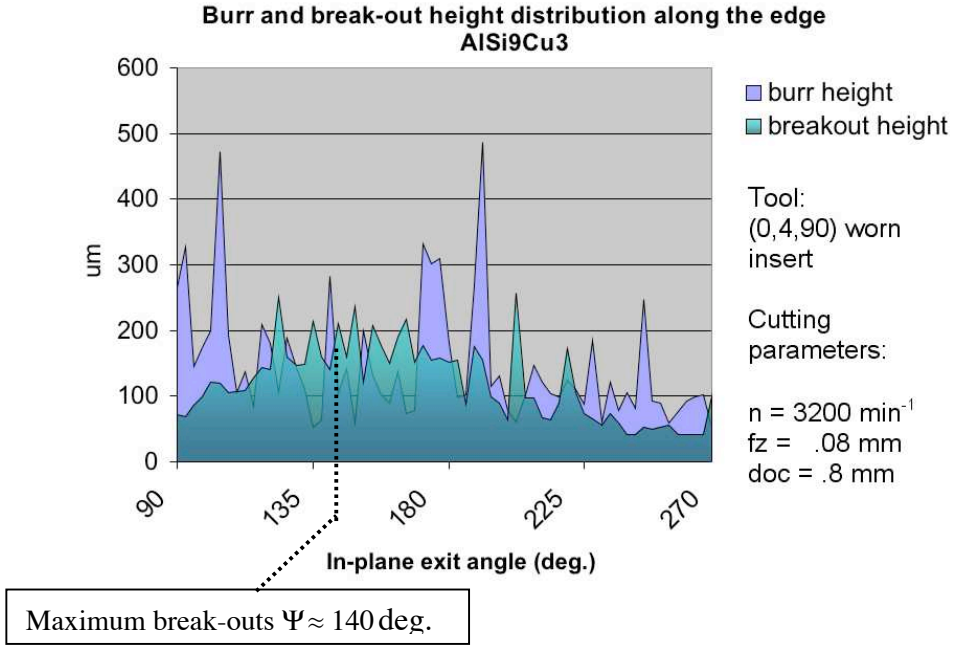

Figure 8. Burr and break-out height of AlSi9Cu3 milled with tool geometry (0,4,90), as a function of in-plane exit angle.

maximum break-out size was observed at approximately 140° in-plane exit angle. This result can be explained by the variation in cutting forces at different in-plane exit angles. Figure 9 depicts the cutting force distribution along the edge as the mill normally exits the workpiece [5]. The maximum cutting forces occur at 140° in-plane exit angles (corresponding to 50° exit angle as defined in [5]), and more severe edge-breakouts are

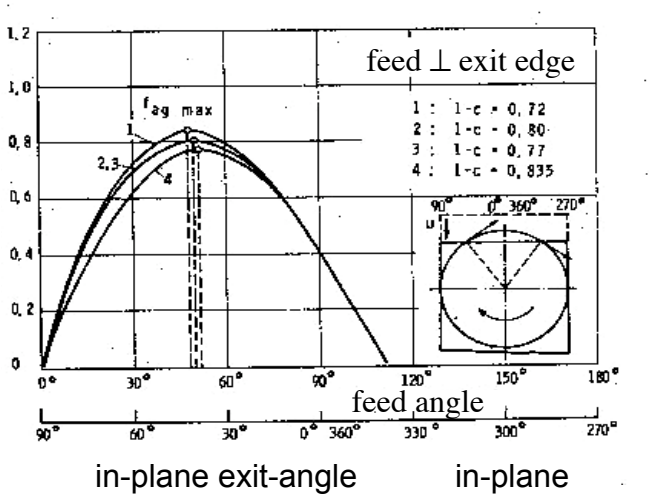

Figure 9. Cutting forces as a function of in-plane exit angle. Tool path is normal to the edge. From Schäfer, 1975 [5].

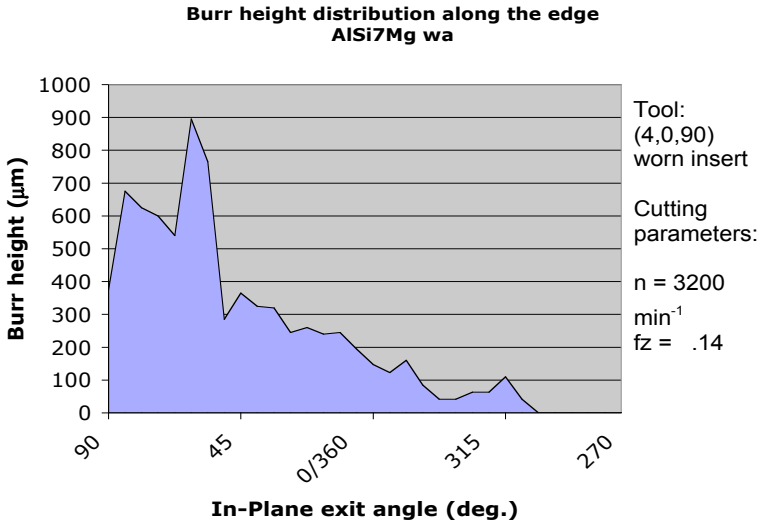

Figure 10. Burr and break-out height of AlSi7Mg-wa milled with tool geometry (4,0,90), as a function of in-plane exit angle.

observed in this region. On the other hand, burr height tends to decrease as in-plane exit angle decreases; this trend was more pronounced in AlSi7Mg wa (Figure 10). This result does not agree with Exit Order Sequence prediction, and it can be explained by the variation in uncut chip thickness at different in-plane exit angles. As the tool gets close to 90° in-plane exit angles, chip thickness becomes very thin. If chip thickness is too thin, the material will be more likely to plow and cutting is more difficult. Under these circumstances, burrs are more likely to occur, and that explains why the tallest burrs were observed in this region. To prove this hypothesis, variable feedrate milling tests with constant uncut-chip thickness at tool exit were performed. A schematic showing the basic relationships is presented in Figure 11. Figure 12 shows a comparison between conventional milling and constant-chip (variable feed) milling. A 50% reduction in burr

height was obtained, and the burr height distribution along the edge does resemble EOS prediction.

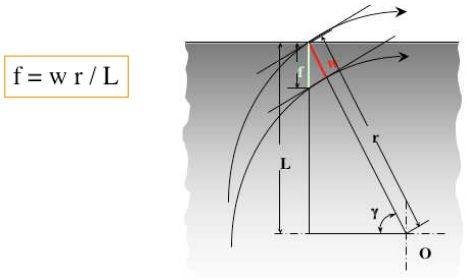

Figure 11. Variable feed test relations.

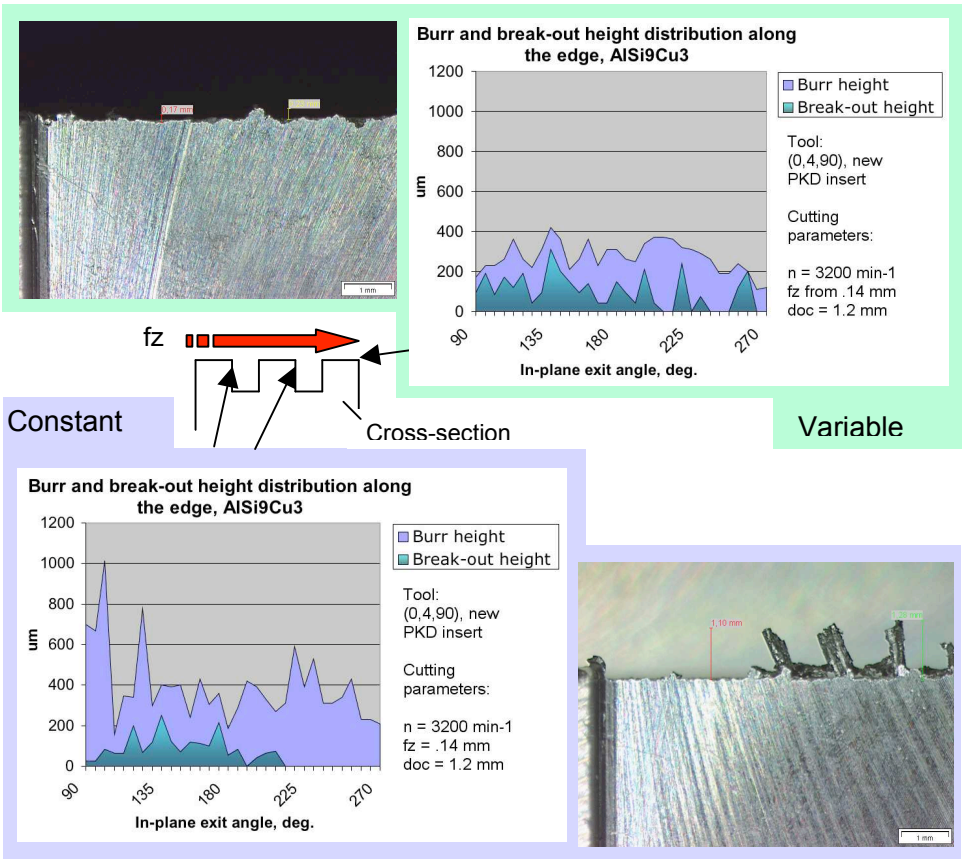

Figure 12. Variable feed test results.

3.5. Effect of tool geometry in burr and break-out height

Figure 13 shows the results of exit burr, exit break-out and entrance burr height as a function of tool geometry on AlSi9Cu3 alloy. Tool geometry (0,4,90) produced, in average, the smallest exit burrs, in spite of forming the largest burrs at a cutting speed of 2513 m/min. The second smallest exit burrs were produced by tool geometry (4,0,90). It

is to note that exit burr height for the different tool geometries (averaged across all cutting conditions) did not differ more than 20%. This difference is not particularly significant; however, in terms of entrance burr height and break-out height, the differences were more substantial. Tool geometry (0,4,90) induced entrance burrs about 10 times taller than those created by the other tool configurations. Similarly, exit edge break-outs were about 5 times larger. This observation can be explained by the greater cutting pressures in the vicinity of the machined surface, associated with a neutral axial rake angle. Consequently, brittle failure and crack propagation are induced in this area. Overall, tool geometry (4,0,90) represents the best alternative for burr minimization on AlSi9Cu3.

The effect of tool geometry in exit burr and entrance burr height on the more ductile alloy, AlSi7Mg-wa, is presented in Figure 14. As with AlSi9Cu3, the different geometries didn't produce important variations in exit burr height, but significant differences were observed in entrance burr size. In this case, the best tool geometry is (0,4,90).

The observed tool geometry effect on burr height did not follow EOS prediction. A plausible explanation for this is that the nose chamfer of the PKD insert (Figure 3, 0.41 mm), is quite large compared to the feeds per tooth used (0.08 and 0.14mm); thus, the tool can not be considered sharp as assumed by EOS theory. Material properties have a strong effect in burr size as well. This is put in evidence by the entrance burr size results. Tool (0,4,90) produces the smallest entrance burrs in the more ductile material, AlSi7Mg-wa, and produces the biggest entrance burrs in the more brittle material, AlSi9Cu3. A better understanding of the 3-dimensional interaction between axial and radial rake angles, depth of cut to uncut chip thickness aspect ratio, nose radius and brittle-ductile material behavior transitions is necessary to design more reliable burr size prediction algorithms.

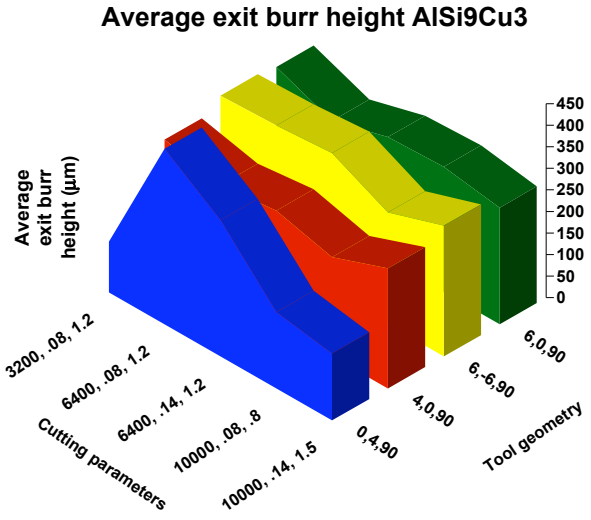

(a)

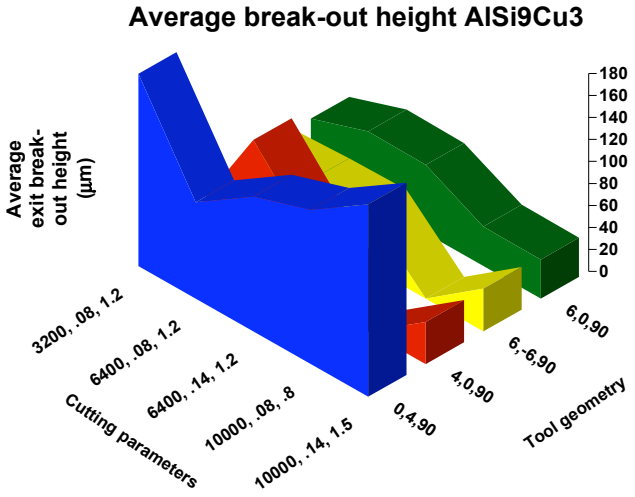

(b)

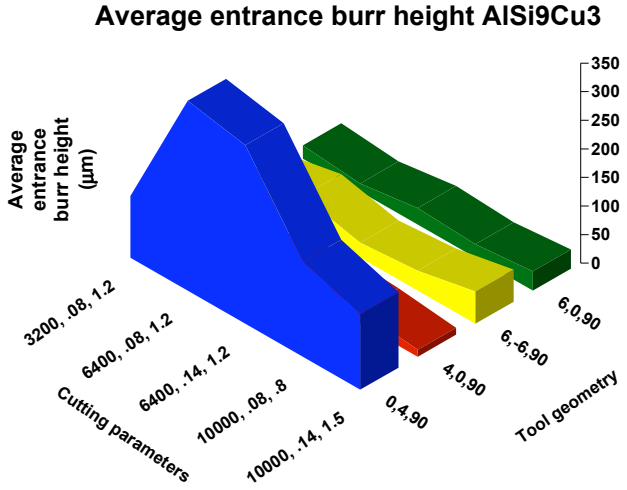

(c)

Figure 13. Exit burr (a), exit break-out (b), and entrance burr height (c) of AlSI9Cu3 as a function of tool geometry and cutting conditions.

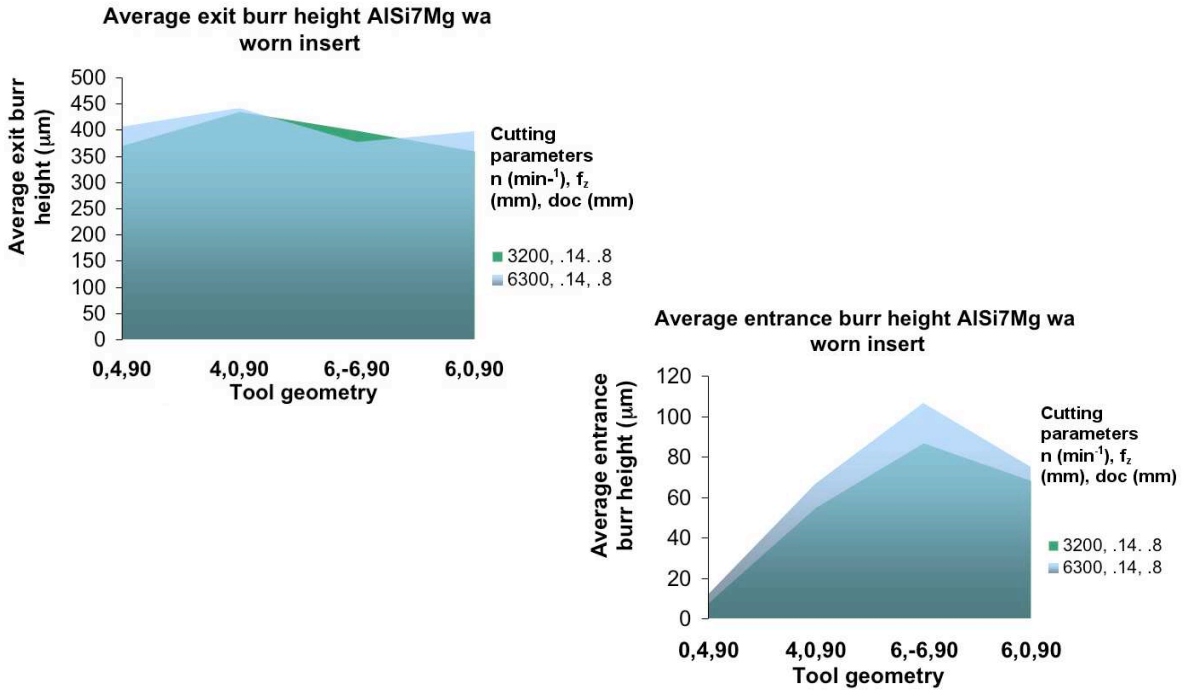

Figure 14. Exit burr and entrance burr height of AlSi7Mg wa as a function of tool geometry and cutting conditions.

4. Conclusions

The following conclusions epitomize the results of the face milling experiments on AlSi9Cu3 and AlSi7Mg-wa alloys:

- Tool geometry (4,0,90) induces the smallest burrs and break-outs on AlSi9Cu3.
- On AlSi7Mg-wa, tool geometry (0.4.90) produced the smallest burrs.
- On brittle materials, the increase in burr push-out force at 140° in-plane exit angle translates into bigger edge break-outs.
- The transition from ductile to fragile cutting regime on AlSi9Cu3 occurs at a cutting speed of approximately 2500 m/min. Overall, the largest burrs on both alloys were recorded under this regime.
- When uncut chip thickness decreases, due to a decrease in the angle formed by in-plane tool exit and feed directions, exit burr size increases. Under these circumstances, an increase in feedrate can reduce burr size by 50% by keeping uncut-chip thickness constant.

References

[1] Hashimura, M., Hassamontr, J., Dornfeld, D., "Effect of In-Plane Exit Angle and Rake Angles on Burr Height and Thickness in Face Milling Operation", *ASME J. of Manufacturing Sc. And Eng*., 121, 13 (1999).

[2] Bansal, A., and Lee, K., "Study of Burr Size and Surface Roughness in High Speed Face Milling", *2001-2002 LMA Annual Reports*, UC Berkeley.

[3] Bansal, A., "Comprehensive approach to Burr Prediction", *2001-2002 LMA Annual Reports*, UC Berkeley.

[4] Gillespie, L.K., *Deburring and Edge Finishing Handbook*, SME, 1999.

[5] Schäfer, F., *Entgraten Theorie Verfahren Anlagen*, Mainz Krausskopf Verlag, 1975.

[6] Nakayama, K., and Arai, M., "Burr Formation in Metal cutting", *Annals of the CIRP*, Vol. 36, No. 1, 1987, pp.33-36.

[7] Kishimoto, W., Miyake, T., Yamamoto, A., Yamanaka, K., and Takano, K., "Study of Burr Formation in Face Milling", *Bulletin Japan Society of Precision Engineering*, Vol. 15, No. 1, 1981, pp. 51-53.